Article:
Pesce, C., Godina, M.C., Henry, A. et al. (2021) Towards a better understanding of hot-mixed mortars for the conservation of historic buildings: the role of water temperature and steam during lime slaking. Heritage Science, 9 (1). 72. ISSN: 2050-7445

https://doi.org/10.1186/s40494-021-00546-9

Pesce *et al. Herit Sci* (2021) 9:72
https://doi.org/10.1186/s40494-021-00546-9

Heritage Science

RESEARCH ARTICLE Open Access

Towards a better understanding of hot-mixed mortars for the conservation of historic buildings: the role of water temperature and steam during lime slaking

Cecilia Pesce[1], Martha C. Godina[1], Alison Henry[2] and Giovanni Pesce[1*]

Abstract

According to various historic accounts and material evidence, the practice of producing lime mortars by mixing the quicklime with the sand (i.e. hot-mixing) before first slaking it with water was much more common in the past centuries than appreciated by most contemporary academics, conservation professionals and craftsmen. However, in the last 10 years, there has been resurgence in interest in hot-mixing. In such systems, the steam developed during the mixing is supposed to be crucial in determining the superior characteristics of the mortars, but in-depth investigations on the role of steam in hot-mixing are very few. This study reports the results of some experimental work investigating the effects of water temperature and steam used for lime slaking on the characteristics of lime and related mortars. In these tests, calcic quicklime was slaked in water at 20 and 75 °C, and with steam at 90 °C. Microstructure and mineralogical characteristics of the hydrates were characterized by scanning electron microscopy (SEM) and X-ray diffraction (XRD). Mortars produced with these limes were tested for fresh (water retention and flowability) and hardened (compressive and flexural strength) properties. Carbonation was assessed using SEM, XRD and phenolphthalein tests. Results show that steam-slaked lime is characterised by portlandite crystals with smaller crystallite size and significantly different microstructure compared to that of water-slaked lime. Results also show that mortars made with steam-slaked lime have higher water retention and flowability than the mortars produced with water-slaked lime. Under conditions of comparatively low relative humidity (c 40–50%), carbonation is slower in the steam-slaked lime mortar due to the lower water content compared to water-slaked lime mortars. Overall, these results confirm anecdotal reports of better workability and water retention and suggest that this production technology, which is only rarely used nowadays, can produce mortars with improved characteristics, and provide a means by which to match the performance of some historic mortars, and create compatible materials for conservation and restoration work.

Keywords: Hot-mixed lime mortar, Water retention, Water demand, Mechanical properties, Steam slaking

Introduction

Recent years have seen a growing interest in a traditional method of mortar production, generally referred to as 'hot-mixing', that was widely used in the past but is only used nowadays by a few specialists [1–3]. Such technological process differs from the more common 'wet' mix in the fact that quicklime is mixed with sand without being first slaked with water. Although slightly different approaches can apply to this production process, the basic method is essentially the same across the world and throughout time. What makes this technology 'different' is the fact that the slaking is achieved through the moisture of the sand, first, and only subsequently by adding

*Correspondence: giovanni.pesce@northumbria.ac.uk
[1] Department of Architecture and Built Environment, Northumbria University, Newcastle upon Tyne NE1 8ST, UK
Full list of author information is available at the end of the article

just enough water to bring the mixture to a workable mortar [4, 5].

The increasing interest in hot-mixing within the conservation industry is demonstrated by the growing number of events such as conferences, workshops, training courses and public demonstrations organised over the past years on this topic (e.g. events organised by the Building Limes Forum and by the Scottish Lime Centre in the UK), that have attracted hundreds of attendees and much attention from specialists. Furthermore, several contractors currently offer the use of hot-mixed mortars in conservation and restoration projects. Within the conservation industry, hot-mixed mortars find application in brickwork, rubble masonry, wall cores, and bridge construction, as well as in finishes such as hot limewashes and sheltercoats [1, 4].

Hot-mixed mortars carry high historic relevance. According to the work of Schmidt [6], who analysed the database of over 3500 historic mortar samples of the Scottish Lime Centre Trust, hot-mixed mortars comprised over 80% of all mortar samples dating from before the 17th century, more than 60% of samples dating from the 17th to the 19th century. Even in the early 20th century, when the use of lime mortars started to phase out in favour of Portland cement mortars, hot-mixed mortars were far more common than putty-based mortars. Furthermore, more and more peer-reviewed papers focused on the analysis of historic mortars suggest the use of this technology in the past centuries, such as in the case of the 16th century mortars used in the Amaiur Castel (Navarre, Spain) [7] and medieval wall painting plasters in Denmark [8].

The advocates of hot-mixed mortars suggest that these mixes outperform the mortars made with lime putty in terms of workability, durability and costs (i.e. are cheaper to produce). Further claims suggest that hot-mixing improves the bond between lime and aggregate; that the development of steam may create an altered pore structure that facilitates the carbonation reaction and enhance the durability of the mortars; that aggregates of a wider range of dimensions are efficiently held in suspension (i.e. reduced gravity segregation), easing the application of the fresh mix [1, 4]. However, none of these claims has been scientifically proved yet, since all these benefits are exclusively evaluated on an empirical basis and interpreted by unproved technical explanation.

A possible reason for the uncertainty surrounding this technology is the very little technical literature available on it. This includes the Technical Paper 28 published by Historic Environment Scotland [5], a book chapter written by Alan Foster in the book: '*Building Limes in Conservation*' [2], a journal article published by the same author in the Journal of Architectural Conservation [1], a short paragraph in the book '*Practical Building Conservation: Mortars Renders and Plaster*' published by English Heritage [9], and a recent book written by Nigel Copsey [4]. Even less is available within the scientific literature: Margalha et al. [10] asserted that the hot-mixing method has positive effects on flexural and compressive strength, cracking susceptibility and capillary water absorption of mortars. The results of an investigation of historic hydraulic mortars prepared by hot-mixing led by Moropoulou et al. [11] allowed the authors to state that this production technology (and the raw materials used) imparted high strength to the mortars. In a study by Valek et al. [12], the authors compared properties of hot-mixed mortars with those of mortars prepared with lime putty and commercial dry hydrate and found that hardened properties of the mortars were comparable across the production methods, whereas the hot mix had higher porosity and higher capillary absorption capacity than the 'cold-mixed' mortars. However, none of these studies has been able to unravel the relationship between the changes induced in the lime by different slaking processes and the improved characteristics of the mortars, a fundamental step in understanding the mechanisms underlying this technology.

An important aspect that deserve attention for advancing our understanding of the properties of hot-mixed mortars, is the role that steam plays in hot-mixed technology, as highlighted in a recent publication by Copsey [4]. Considering the descriptions available in the literature [4] and the practical experiences of some of the authors, it has been inferred that in the "hot-mixed" system the slaking process of lime (CaO) is likely to take place through two steps: in the first, the water adsorbed on the surface of the sand grains in contact with CaO reacts with the CaO initiating the slaking. Because of the heat produced during this reaction, the water adsorbed on the surface of the surrounding sand grains is subsequently converted to steam that diffuses through the pores in between the sand grains and promotes the slaking of further unreacted CaO (step 2). If this is the case, the effects of steam slaking on portlandite crystals is an essential aspect of hot-mixed mortars that has never been investigated in detail. Studies that partly investigate this effect have been carried out in other research areas such as in the desulphurization process of industrial emissions. In such context, vapour hydration of CaO is a process commonly used to produce high-performance CO_2 sorbents [13, 14]. The vapour hydration reaction mechanism was firstly investigated in 1964 by Ramachandran [15] and later confirmed by Beruto et al. [6], who suggested that a different path is followed when CaO is slaked by liquid water then when slaked by steam. In the former case, a

liquid-state homogeneous dissolution/re-precipitation process occurs, whereas in the latter case a solid-state topotactic reaction takes place. As a result, $Ca(OH)_2$ formed by steam slaking is made up of a fine, poorly crystalline phase which can rapidly react with CO_2 [13, 14]. Our recent preliminary work [17] shows that portlandite formed by CaO vapour hydration exhibits different mineralogical features from portlandite precipitated by CaO in solution.

This study aims at investigating the characteristics and properties of lime when subject to slaking under conditions similar to those in the hot-mixing technology—under a heap of moist sand, in a receptacle very rich in steam—by recreating such conditions in a simplified system under controlled temperature and humidity. This is achieved by: (i) slaking Ca-rich quicklime in different conditions (steam and water at various temperatures) and analysing the mineralogy and microstructure of the obtained slaked limes, and (ii) testing some of the properties of mortars prepared with the lime produced. It is worth noting that mixing steam-slaked lime with sand does not necessarily produce a mortar with the same properties as a hot-mixed mortar, nor this study was aimed at producing a hot-mixed mortar. However, it is important to stress that, although this research focuses on the characteristics of steam-slaked lime rather than of the hot-mix mortars, its results can be used to broaden our knowledge of the hot-mixed mortars. In fact, the outcome of this investigation provides insights on what is regarded by practitioners and most literature as an essential factor in determining the advantageous properties of hot-mixed lime mortars: the presence of vapour as one of the main phases of the slaking process. Since hot-mixed mortars are increasingly used in conservation works, where they seem to outperform putty-based mortars and a like-for-like approach is often sought, it is vital to gain scientific knowledge on this technology.

Materials and methods

Raw materials

The quicklime used in all experiments was Calbux Fine 6 (0–6 mm high reactivity quicklime) from Tarmac Buxton Lime and Cement. The aggregate used in mortars was a silica sharp sand as defined by the producer (Chas Long & Son Aggregates, Richmond, UK), granulometry 0–4 mm. The raw materials were characterised in terms of density and grain size distribution. The skeletal density was measured with a Micromeritics AccuPyc II 1340 helium pycnometer; the grain size distribution was measured by dry sieving according to the standard BS ISO 11277:2020 [18]. The results are shown in Table 1 and Fig. 1.

Lime slaking

To investigate the effect of steam-slaking and water slaking at different temperature on the microstructural and mineralogical characteristics of lime, 3 different batches of slaked lime were produced by slaking the same quicklime in different conditions (Table 2). Lime 'A' was produced at room temperature as a 'control' slaking process and, therefore, to be used as a reference for evaluating any differences observed in the other batches of lime as a result of slaking at higher temperature. For producing lime 'A', the quicklime was mixed with de-carbonated deionised (DI) water in 1:3 $CaO:H_2O$ mass ratio, as indicated by other authors for the preparation of lime putty [19–23]. The water was poured all at once onto the quicklime in a metal bucket and, immediately after the initial vigorous bubbling, hand-mixed for at least 10 min. When the temperature reached again the environmental conditions, samples of the obtained putty were collected and dried in a desiccator for at least 24 h for characterisation. The remaining content was stored in excess of DI water, inside airtight containers until mortar production.

Lime 'B' was produced to investigate the effect of the water temperature on the characteristics of lime. For

Table 1 Grain size distribution and density of the raw materials

CaO				Sand			
Sieve aperture size (μm)	Retained mass proportion %	Cumulative retained mass proportion %	Skeletal density (g/cm^3)	Sieve aperture size (μm)	Retained mass proportion %	Cumulative retained mass proportion %	Skeletal density (g/cm^3)
63	1.76	1.76	2.88	63	2.96	2.96	2.70
106	3.26	5.02		106	0.29	3.25	
212	2.04	7.06		212	11.36	14.61	
250	3.38	10.45		250	13.39	28.00	
500	88.93	99.38		500	19.37	47.37	
				1000	22.73	70.10	
				2000	25.56	95.66	

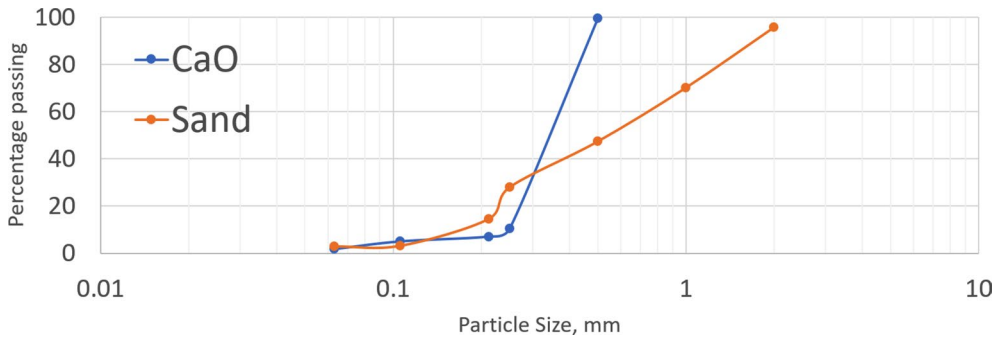

Fig. 1 Cumulative grain size distribution chart of the raw materials

Table 2 Slaking conditions and mortar preparation

Sample name	Lime slaking			Mortar preparation	
	Slaking conditions	T slaking water (°C)	Lime form	Binder:aggregate (v:v)	w/b ratio (w/w)
A	Water	20	Putty	1:3	–
B	Water	75	Putty	1:3	–
C	Steam	–	Dry hydrate	1:3	0.6

producing lime 'B', the quicklime and de-carbonated DI water were separately heated in an oven until they reached 75 °C. Subsequently, the quicklime and the water were mixed in a mass ratio 1:3 CaO:H_2O, in a similar way to the lime 'A'.

Lime 'C' was produced to investigate the effect of steam slaking on the characteristics of lime. For producing lime 'C', the quicklime was crushed and sieved to obtain particles with ø < 500 µm. The quicklime was then placed in an oven together with open beakers filled with de-carbonated water at 90 °C, so that steam was produced but water did not reach boiling point and so the spilling of liquid water into the CaO tray was prevented. The quicklime was left to slake in the oven for 8 h. Figure 2 shows the experimental setup and the visible volumetric expansion of the lime that occurred as a result of slaking. At the end of the test, samples of lime were collected and dried in a desiccator for at least 24 h prior to characterisation. The remaining lime was sealed inside airtight containers until mortar production.

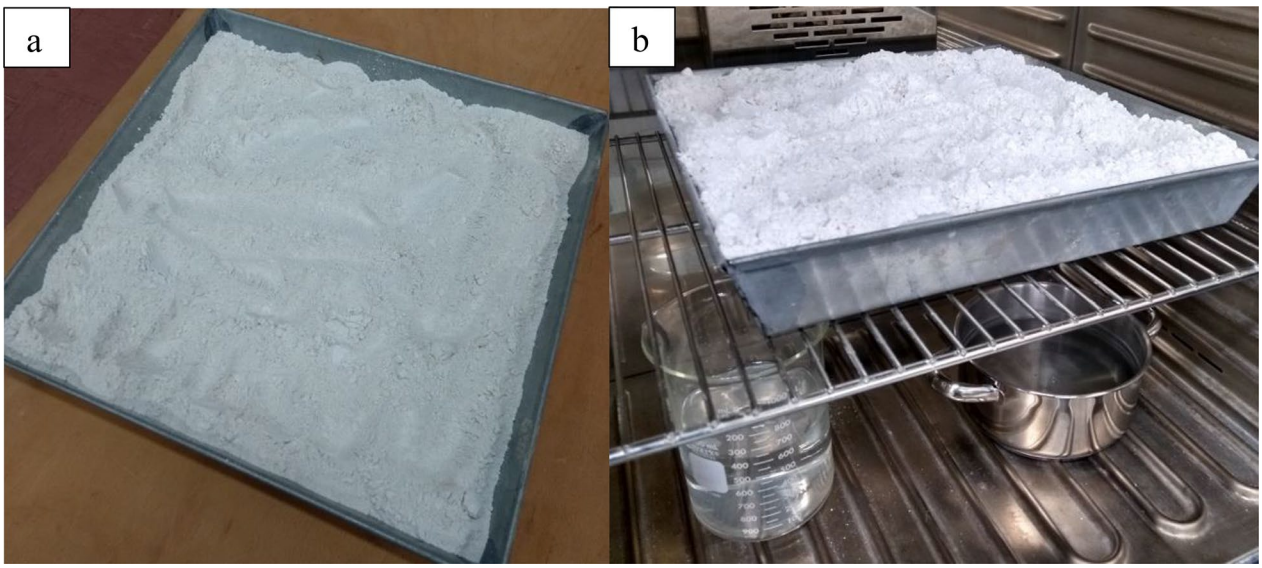

Fig. 2 Set up of the steam-slaking experiment. **a** Quicklime particles before the slaking. **b** Lime particles at the end of the slaking process

Mortar preparation and curing conditions

The slaked limes obtained as described in Sect. "Lime slaking" were used to produce mortars as described in Table 2. Each batch of lime was mixed with silica sand using a binder-to-aggregate (b:a) ratio of 1:3 v/v. All mortar mixtures were mechanically combined with a laboratory mixing equipment (a planetary mixer similar to the mixer specified in EN 196-1 [24] for 15 min. In the case of water-slaked limes (A and B), the lime putty was mixed with sand without adding further water. In the case of steam-slaked lime, which was in the form of a powder, firstly the hydrated lime was combined with sand in the mixer, and subsequently DI water was added gradually to the mix until reaching a w/b ratio of 0.6 w/w to obtain a workable consistency.

The moulding of the mortars was carried out manually by compacting the mortar using a metal rod. The samples were cast in two layers, tamping firmly the mortar surface in a uniform manner with ~ 25 strokes each layer. Two different types of mould were used for testing:

1. *Plastic cylinders of 30 mm diameter × 50 mm height for microstructural and mineralogical characterisation and phenolphthalein test.* Twenty-four samples were produced for each batch of lime in order to obtain 3 replicas at each pre-set age of: 15, 16, 17, 20, 21, 28, 35, 42 days of curing. The time points were selected in order to allow the samples to be safely demoulded, and to closely monitor the evolution of the samples at early ages (within one week from demoulding) and at mid-term on a weekly frequency, in addition to the standard curing times usually selected in studies of hydraulic binders.
2. *Prismatic specimens of 40 × 40 × 160 mm for flexural and compression tests.* All specimens were cured inside the mould for 14 days in laboratory conditions (~ 20 °C, 50% relative humidity [RH]) after which they were demoulded. Four replicas were produced per batch of lime and testing was carried out after 28 days of curing.

Characterisation methods

The microstructural and mineralogical characteristics of the quicklime and slaked limes were investigated using scanning electron microscopy (SEM) and X-ray diffraction (XRD) analyses. Chemical, microstructural and mineralogical characteristics of mortars were investigated using phenolphthalein, SEM and XRD.

Fresh-state properties (water retention and water demand) and hardened-state properties of mortars (flexural and compression tests) were measured to investigate the effect of the slaking process on their characteristics.

Scanning electron microscopy

The microstructural characteristics of the quicklime, slaked lime and mortar samples were investigated using a Tescan Mira 3 SEM in high-vacuum mode and gun voltage of 10 kV. Quicklime samples were fixed on a metal stub with carbon tape and sputtered with a 5 nm thick layer of platinum to make the analysed surface conductive. The samples of slaked lime were dried in a vacuum oven for 6 h and then fixed on a metal stub with carbon tape and platinum coated. For the mortar samples, a freshly cut sub-sample was removed from the core of 3 cylinders of each age (described in Sect. "Mortar preparation and curing conditions"). The fragments were then mounted on a metal stub with carbon tape and platinum coated. Since sample preparation took place at low RH (~ 30%), it is possible to assume that during this time, no significant carbonation occurred.

X-Ray diffraction

The mineralogical characteristics of the quicklime, slaked lime and mortar samples were investigated using a Rigaku SmartLab X-ray diffractometer (Cu-K_α radiation, parallel beam geometry, 2 − θ range 10–90°, step 0.05°, scan speed 1.5°/min, 40 kV, 50 mA). Phase identification, quantitative phase analysis and crystallite size evaluation were carried out using the Rigaku SmartLab Studio II software. The crystallite size was calculated using the Hall's method implemented in the same software [25]. Prior to XRD analysis, quicklime and slaked lime samples were ground with an agate pestle and mortar, sieved to < 63 μm, and mixed with 10% w/w zincite used as internal standard for quantification of possible amorphous phases.

For each pre-set mortar age, one of the 3 cylindrical samples was chisel-cut to obtain a central 2 cm thick slice, which was then crushed using a hammer until particle size was < 5 mm. From the crushed material, a sub-sample was selected using the coning and quartering method. The sample obtained was then finely crushed with an agate pestle and mortar to a < 106 μm granulometry.

Phenolphthalein test

To provide visual evidence of the carbonation front, the phenolphthalein test was carried out on all the cylindrical samples at each age, according to the British Standard BS EN 14630 [26]. The phenolphthalein was sprayed onto the surface of two longitudinal halves of the cylinders, obtained by splitting them with a chisel. The stained surfaces were photographed immediately after spraying.

Water retention

The water retention of fresh mortars was investigated using the method detailed in the British Standard BS EN 459-2:2010 [27], previously used by other researchers [28], and the testing equipment provided by Novanna Measurement Instrument (product code 1.0246). In these tests, freshly-mixed mortars with known water fraction are put in contact with a filter plate, simulating the action of an absorptive substrate. To calculate the water retention of the fresh mortars, 3 samples of each batch of lime were tested in order to acquire statistically meaningful data.

According to BS EN 459-2:2010, the water fraction (W_1) of the mortars is calculated as in Eq. (1) where m_{21} is the total mass of water in fresh mortar (g) and m_{22} is the mass of dry mortar (g).

$$W_1 = \frac{m_{21}}{m_{21} + m_{22}}. \quad (1)$$

The water content of the tested samples of mortar (W_2) was defined as in Eq. (2):

$$W_2 = m_{23} \times W_1, \quad (2)$$

where m_{23} is the mass of the tested sample of mortar (g). The mass of water absorbed by the filter plate (W_3) was defined as in Eq. (3):

$$W_3 = m_{20} - m_{17}, \quad (3)$$

where m_{20} is the mass of the soaked filter plate (g), and m_{17} is the mass of the dry filter plate (g). The relative loss of water from the mortar (W_4) was defined as in Eq. (4).

$$W_4 = \frac{W_3}{W_2} \times 100. \quad (4)$$

The water retention capacity (WR) of a freshly-mixed mortar was calculated as a percentage according to Eq. (5).

$$WR = 100 - W_4. \quad (5)$$

Water demand

The water demand of fresh mortars was evaluated through the consistency of the mix, measured by flow table test as in BS EN 459-2:2010 [27] and BS EN 12350-5:2019 [29]. This apparatus determines the consistency of the fresh mortars by measuring their spread on a horizontal flat plate which is subjected to jolting. Results are reported as the average obtained by measuring the minimum and maximum dimension of the mortar spread and are reported to the nearest 10 mm. To evaluate the consistency of the mortar produced with water-slaked lime (batch A and B), mixtures were produced without adding any water, whereas to evaluate the consistency of the mortar produced with steam slaked lime (type C), various amounts of water were added until the mortar samples achieved a similar spread to those containing lime putty. This also allowed evaluating water quota to add to the mixtures produced using steam-slaked lime in order to reach an appropriate workability as required for water retention test. To obtain a statistically significant value of the spread in mortars produced with lime putties, 3 tests were carried out for each mix.

Mechanical tests

Hardened-state properties of the same mortars prepared for the water demand test (previously described in Sect. "Water demand") were measured after 28 days of curing. Flexural and compression tests were carried out using an INSTRON 3382 Floor Model Universal Testing System with loading cell of 100 kN capability, and load accuracy of 0.5% of the indicated load, as described in the British Standard BS EN 196-1:2016 [24].

Flexural tests were carried out on the prismatic samples described in Sect. "Characterisation methods". Table 3 reports the geometrical characteristics of the samples tested. Flexural strength was evaluated using the three-point loading method. Load rate was 0.2 mm/min, and the distance between the two supports was 100 mm. Flexural strength (R_f, in megapascals) was calculated according to Eq. (6) where F_f is the load applied to the middle of the prismatic sample at fracture in newtons; b is the width of the tests sample in millimetres; h is the thickness of the tested sample, in millimetres; l is the distance between the supports, in millimetres.

Table 3 Width (b), thickness (h) and cross-sectional area of the prismatic samples tested for flexural strength at 28 days

Mortar sample	*b* (mm)	*h* (mm)	Area (mm^2)
Lime type A-1	39.62	39.81	1577.27
Lime type A-2	39.08	38.25	1494.81
Lime type A-3	39.25	38.2	1499.35
Lime type A-4	39.24	39.4	1546.06
Lime type B-1	38.35	39.19	1502.94
Lime type B-2	39.19	39.44	1545.65
Lime type B-3	38.42	39.47	1516.44
Lime type B-4	38.44	39.24	1508.39
Lime type C-1	39.11	38.84	1519.03
Lime type C-2	37.46	37.01	1386.40
Lime type C-3	39.46	39.37	1553.54
Lime type C-4	39.42	39.02	1538.17

$$R_f = \frac{1.5 \times F_f \times l}{b \times h^2}. \quad (6)$$

Compressive test was carried out on the broken halves of the prismatic samples used in the flexural test. Compressive strength was evaluated using the same load rate of 0.2 mm/min and calculated using Eq. (7) where R_c is the compressive strength, in megapascals; F_c is the maximum load at fracture, in newtons; b is the width of the tests sample in millimetres; h is the thickness of the test sample in millimetres.

$$R_c = \frac{F_c}{b \times h}. \quad (7)$$

Compressive and flexural strength values reported in paragraph Sect. "Flexural and compressive tests" are the mean values of the measurements on the four replicas of each lime mortar sample. Error bars represent confidence intervals at 90% and were calculated with the following formula [30]:

$$\pm t_{n-1} \frac{s}{\sqrt{n}}, \quad (8)$$

where t_{n-1} is the Student's t-score reflecting a confidence level of 90% (=1.96) at $n-1$ (=3) degrees of freedom, s is the sample standard deviation, and n is the sample size (=4).

Results and discussion

Microstructural and mineralogical characteristics of limes

Figure 3 shows SEM images of the quicklime and the three batches of lime analysed. The quicklime (Fig. 3a) is characterised by a regular microstructure of interconnected particles with heterogeneous sub-rounded pores of about 0.1 μm in diameter. The observed morphology is typical of calcined carbonate minerals [31, 32]. The pore diameter observed by SEM is included in the range of values measured in literature for other calcined limestones [33], although it should be noted that there are several factors that can contribute to the microstructure of the calcined material, including the morphology of the parent material and the calcination conditions [31, 33–35].

The microstructure of the control putty (batch A) slaked at 20 °C (Fig. 3b) displays partially agglomerated crystals of a wide variety of habits and size. Most portlandite crystals have size up to 1.5 μm and display well-developed hexagonal {00.1} faces, with habits varying from platelets, short prism and rod-like. Such crystals are embedded in a matrix of smaller (10–100 nm) crystals showing a granular habit with less regular crystal facets. Pores have diameters of various sizes ranging from few nm to 0.5 μm.

The microstructure of the putty slaked with water at 75 °C (batch B) (Fig. 3c) has pores of various size and shape (ranging from few nm to 0.5 nm, similar to the control putty). Portlandite crystals in batch B have less regular facets than those observed in the control putty. Few μm-sized crystals can be observed, while most crystals are nm-sized and of irregular shape.

The microstructure of the steam-slaked lime (batch C) (Fig. 3d) shows interconnected particles similar to the quicklime and with a similar heterogeneous pore network (pore diameter 0.1–0.5 μm). Although the crystal facets appear mostly irregular, hexagonal thin platelets can be recognised in some of these nm-sized particles. The surface of several particles is characterised by nm-sized cracks.

The diffractograms of the CaO and hydrated lime A, B and C are shown in Fig. 4. The results of phase identification and quantification performed by XRD-Rietveld analysis are reported in Table 4. In the quicklime, CaO is the dominant phase, but minor quantities of portlandite are identified as well. Traces of calcite were found in all lime samples, likely due to reaction with moisture and atmospheric CO_2 during sample preparation. In all slaked limes, portlandite is the dominant phase but some differences can be observed across the three batches of lime.

In the Batch A (lime slaked in water at 20 °C) no trace of original quicklime was found, suggesting that the CaO has fully reacted with water. Conversely, in Batch B (the putty slaked at 75 °C) a small trace (3%) of CaO was identified. This could be due to various reasons: the slaking in hot water results in a more violent reaction than with water at room temperature [36], and the subsequent rapid evaporation of water may have had an effect on some hot spots in the core of quicklime particles that remain unreacted. Another possible explanation is that the rapid evaporation of water increased the actual CaO:H_2O ratio, resulting in the development of hot-spots with high temperatures (e.g. > 200 °C) that may have dehydrated some of the lime that had initially hydrated [36]. In Batch C (lime slaked with steam) most of the quicklime has been hydrated (80% portlandite), but the remaining 20% was unreacted CaO. This was probably due to the limited diffusion of steam within the pores of the pulverised quicklime.

(See figure on next page.)

Fig. 3 SEM images of parent quicklime and of portlandite crystals in limes slaked with the different methods. **a** CaO crystals in quicklime. **b** Lime slaked in 1:3 lime:water ratio at 20 °C. **c** Lime slaked in 1:3 lime:water ratio at 75 °C. **d** Steam-slaked lime. The left and right columns show a low and high magnification, respectively. Insets in **b** and **d** show details of individual crystals

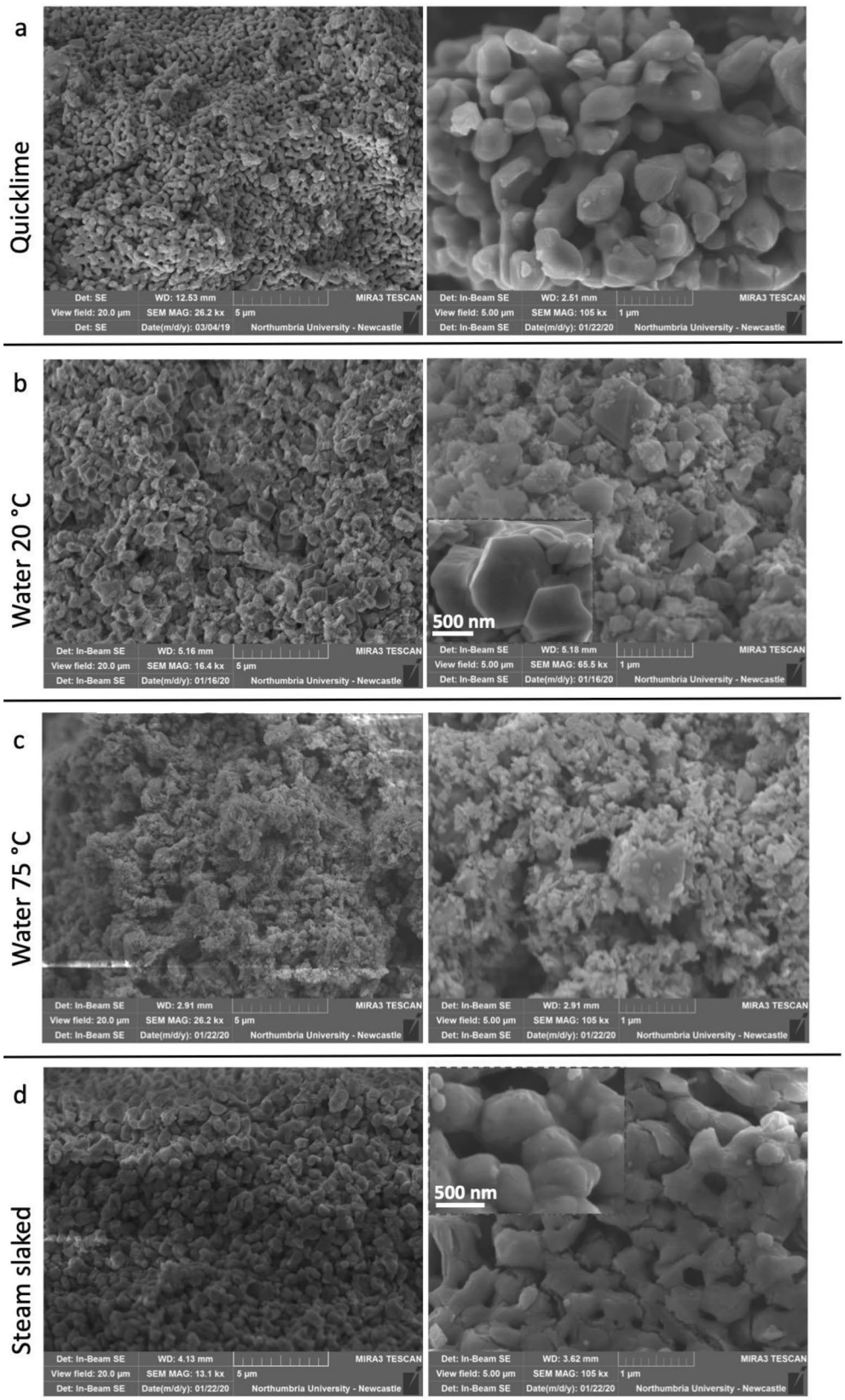
a
Quicklime
Det: SE WD: 12.53 mm MIRA3 TESCAN
View field: 20.0 µm SEM MAG: 26.2 kx 5 µm
Det: SE Date(m/d/y): 03/04/19 Northumbria University - Newcastle
Det: In-Beam SE WD: 2.51 mm MIRA3 TESCAN
View field: 5.00 µm SEM MAG: 105 kx 1 µm
Det: In-Beam SE Date(m/d/y): 01/22/20 Northumbria University - Newcastle
b
Water 20 °C
Det: In-Beam SE WD: 5.16 mm MIRA3 TESCAN
View field: 20.0 µm SEM MAG: 16.4 kx 5 µm
Det: In-Beam SE Date(m/d/y): 01/16/20 Northumbria University - Newcastle
500 nm
Det: In-Beam SE WD: 5.18 mm MIRA3 TESCAN
View field: 5.00 µm SEM MAG: 65.5 kx 1 µm
Det: In-Beam SE Date(m/d/y): 01/16/20 Northumbria University - Newcastle
c
Water 75 °C
Det: In-Beam SE WD: 2.91 mm MIRA3 TESCAN
View field: 20.0 µm SEM MAG: 26.2 kx 5 µm
Det: In-Beam SE Date(m/d/y): 01/22/20 Northumbria University - Newcastle
Det: In-Beam SE WD: 2.91 mm MIRA3 TESCAN
View field: 5.00 µm SEM MAG: 105 kx 1 µm
Det: In-Beam SE Date(m/d/y): 01/22/20 Northumbria University - Newcastle
d
Steam slaked
Det: In-Beam SE WD: 4.13 mm MIRA3 TESCAN
View field: 20.0 µm SEM MAG: 13.1 kx 5 µm
Det: In-Beam SE Date(m/d/y): 01/22/20 Northumbria University - Newcastle
500 nm
Det: In-Beam SE WD: 3.62 mm MIRA3 TESCAN
View field: 5.00 µm SEM MAG: 105 kx 1 µm
Det: In-Beam SE Date(m/d/y): 01/22/20 Northumbria University - Newcastle

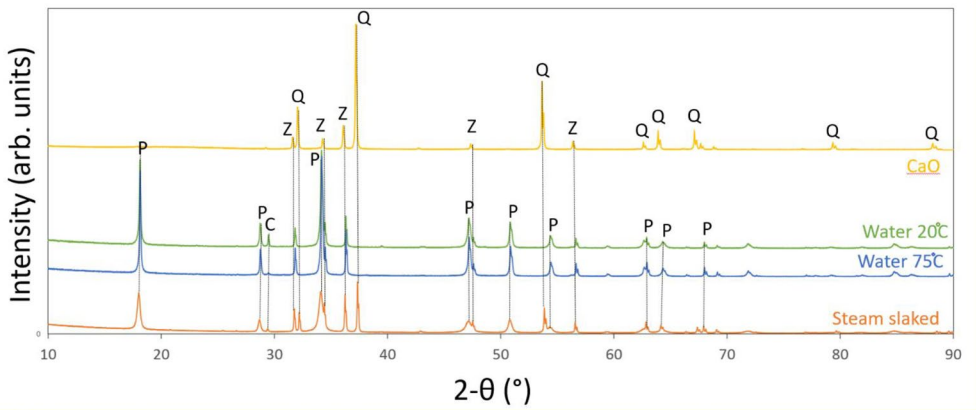

Fig. 4 Diffractograms of the quicklime (yellow plot), of lime A (green plot), lime B (blue plot) and lime C (orange plot). The phases are shown with the following keys: P = portlandite; C = calcite; Z = zincite; Q = calcium oxide

Table 4 Quantitative phase analysis of the lime samples

Sample	CaO (%)	Portlandite (%)	Calcite (%)
Quicklime	94.3	3.4	2.3
Water 20 °C	0	94.5	5.5
Water 75 °C	3.3	95.2	1.5
Steam slaked	19.2	79.1	1.8

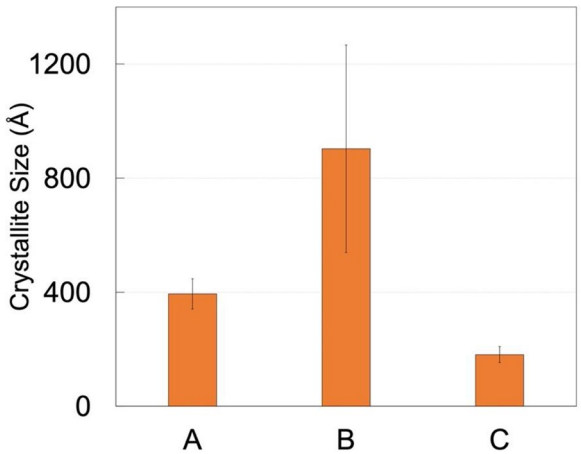

Fig. 5 Portlandite crystallite size calculated from XRD data in the control lime (**a**), in the water-slaked lime at 75 °C (**b**), and in the steam-slaked lime (**c**)

Results of the crystallite size analysis for the various types of lime, calculated from the XRD data are shown in Fig. 5. The graph shows that the steam-slaked lime has significantly smaller crystallites (180 Å) than the water-slaked limes (~ 400–900 Å). The putty slaked in liquid water at room temperature shows crystallite size of 394 Å, whereas the putty slaked at 75 °C shows a bigger crystallite size (900 Å) but also a remarkably higher standard deviation, suggesting that either the crystallites have a wide size distribution or have a high aspect ratio (e.g. plates or needles). Although the SEM micrographs cannot be used as a direct comparison for the crystallite size calculated with XRD (as the lime particles observed by SEM can be aggregates of several crystallites), they can be used for drawing some considerations. In the putty slaked at 75 °C (Fig. 3c) the particles are rather granular and do not show a remarkable high aspect ratio with respect to control lime, which instead display crystals with elongated and plate-like shapes (Fig. 3b). Arguably, it is possible to discard the high aspect ratio hypothesis in favour of the wide crystallite distribution hypothesis, which however should be further verified and investigated.

Overall, the SEM images suggest that the microstructure of the steam-slaked lime is significantly different from that of water-slaked lime. Portlandite crystals formed in the latter samples display a morphology that is commonly encountered in freshly-slaked lime putties [23], whereas the steam-slaked lime reveals a distinct microstructure that resembles that of the CaO. Such remarkable difference can be ascribed to the different conditions in which portlandite crystals are formed upon reaction with water.

Previous studies have shown that well-crystallised $Ca(OH)_2$ forms upon reaction between CaO and liquid water due to the portlandite crystallisation path, via precipitation from a supersaturated solution, and to the subsequent growth enhanced by the rapid diffusion of ionic species in a liquid medium [15, 16]. However, the different microstructure of the steam-slaked lime suggests that hydration took place following a different

reaction path at a gas–solid interface. Without the presence of a liquid phase, diffusion of ionic species—which allows CaO and H_2O to react—is very slow and does not account for the extensive portlandite formation measured by XRD. The reaction path proposed by Beruto et al. [16] involves the diffusion of gaseous H_2O molecules into the CaO phase through the {111} planes of CaO made of O_2^-, which convert upon adsorption of water into {001} planes of $Ca(OH)_2$. However, the distance between {111} planes of CaO is only 2.780 Å whereas the distance between {001} planes of $Ca(OH)_2$ is 4.910 Å and this results in a high anisotropic expansion in the direction normal to the {001} planes. Such mechanism is supported by our SEM images, which show extensive cracks formation (width in the magnitude order of 10 nm) on the surface of the newly formed portlandite (Fig. 3d, right column) likely generated by the stress caused by the volumetric expansion during the conversion from CaO to $Ca(OH)_2$.

Furthermore, the XRD analysis showed that the steam-slaked lime has crystallites of remarkably smaller size than those formed upon water-slaking. This can be explained by considering the mechanism underlying the hydration of CaO by water in vapour phase proposed by Molinder et al. [37]. According to this study, during early hydration $Ca(OH)_2$ nucleates on the {111} planes of CaO, with $Ca(OH)_2$ {001} planes parallel to the CaO {111} planes. However, the Ca-Ca bond length in the CaO {111} plane (3.401 Å) is different from the one in the $Ca(OH)_2$ {001} plane (3.589 Å) and such lattice mismatch induces a significant internal stress in the $Ca(OH)_2$ lattice, which results in failure of the crystal structure and eventually in a small crystallite size.

During vapour hydration, the growth of $Ca(OH)_2$ preferentially occurs in the direction parallel to the {001} planes, as a result of (i) easier diffusion of Ca and O ions from the CaO-core to the $Ca(OH)_2$ surface layer and (ii) easier contact with H_2O molecules [14, 37]. The preferential growth of portlandite along the {001} planes results in crystals with a high aspect ratio (thin platelet shape), as supported by our SEM observations (Fig. 3), which show that in our steam-slaked lime, portlandite mainly exhibits a thin platelet habit, whereas in the other limes (A and B), crystals have thicker, well-developed platelets, short prism, rod-like or granular habits.

It may be argued that during steam slaking, hydration occurs through contact of CaO with liquid water formed by capillary condensation. The minimum radius of the pores in which water can condense can be calculated using the Kelvin equation [38]:

$$r = \frac{2\gamma V_m}{RT\ln(\mathrm{P_0/P})},$$

where r is the pore radius (m), γ is the surface tension of water (0.0608 J/m^2 at 90 °C), V_m is the molar volume of water ($1.8{\cdot}10^{-5}$ mol/m^3), R is the gas constant 8.134 J/(mol K), T is the temperature (363°K), and P/P_0 is the relative vapor pressure of water. Since during the steam-slaking experiment, the reservoir of water had to be periodically refilled, we can assume that inside the slaking chamber, water vapour never reached equilibrium with its liquid phase and hence the humidity was far from saturation. Even assuming a high RH%, e.g. 90%, it is possible to calculate that capillary condensation in such conditions occurs in pores with diameter < 15 nm, which is almost 2 orders of magnitude lower than the pores observed in the SEM images. Thus, the hypothesis that the majority of CaO during steam-slaking was slaked in liquid water by capillary condensation can only apply to a limited pore volume and, consequently, it is possible to assume that most of the hydration during our steam-slaking experiments occurred in the absence of a liquid phase.

Water retention

Results of the water retention (WR) tests are reported in Table 5. The results obtained for the water retention of mortar based on lime A (water-slaked at 20 °C) are in good agreement with WR values reported by other authors for lime mortars [39, 40] and references therein. Water retention of the mortar based on lime 'B' (water-slaked at 75 °C) is closer to the WR of the mortar based on the steam-slaked lime (type 'C') suggesting a possible influence of the slaking temperature on the capability of the mortars to retain water during mixing. The results also show that the mortar containing steam-slaked lime is capable to retain more water than mortars produced using water-slaked lime.

WR values of mortars based on lime 'B' and 'C' are remarkably high and this is likely related to the microstructural characteristics of these types of lime, that

Table 5 Results of water retention tests

Lime Type	Replica n	Water fraction W_2 (g)	WR %
A (20 °C)	1	55.7	87.5 ± 1.2
	2	55.9	
	3	54.1	
B (75 °C)	1	51.3	92.6 ± 1.4
	2	55.8	
	3	54.9	
C (steam-slaked)	1	41.3	96.2 ± 0.8
	2	52.3	
	3	55.4	

are, in turn, consequence of the slaking conditions. The SEM analyses (Fig. 3), in fact, show that lime A is constituted by µm-sized, well-crystallised portlandite, whereas in lime B and C portlandite crystals seem of sub-micrometer granular shape and nm-sized thin platelets, respectively. These morphologies are likely to produce a higher specific surface area than the bigger crystals in lime A. The specific surface area of the binder is known to be positively correlated with the water retention of a mortar [28, 41]. Moreover, the morphologies of limes B and C (particularly the latter), are also likely to be related to a higher colloidal stability [42] and in these systems water is more homogeneously distributed, allowing a higher water retention. In particular, small and plate-like $Ca(OH)_2$ particles (like the ones found in our steam-slaked lime samples) are reported to have higher capacity of absorbing water than bigger, prism-shaped crystals and are thus able to increase the overall water retention of a mortar [42].

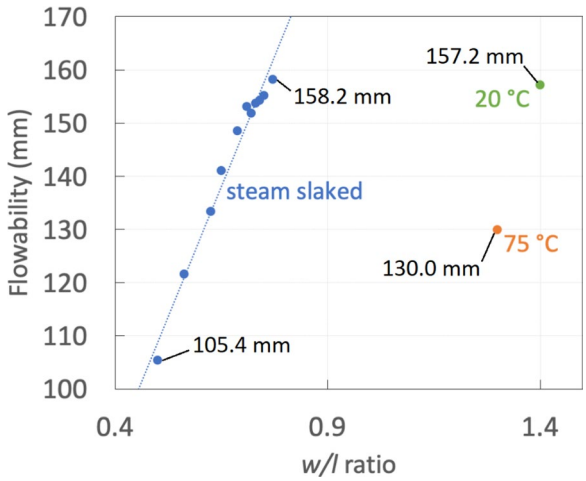

Fig. 6 Plot of flowability vs w/l ratio of mortars based on steam-slaked lime (blue plots and trend line) and on putties water-slaked at 20 °C (green plot) and 75 °C (orange plot)

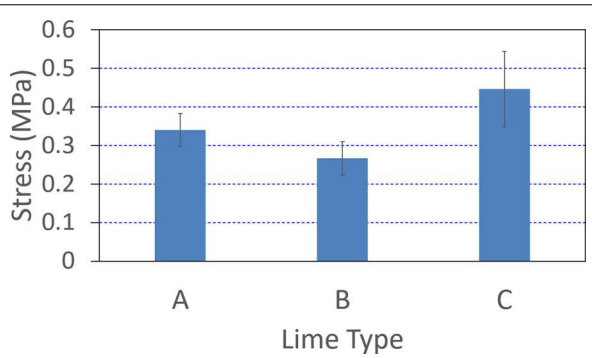

Fig. 7 Bending stress at maximum load at 28 days for the mortars produced with water-slaked lime at 20 °C (**A**) and 75 °C (**B**) and with steam-slaked lime (**C**)

Water demand

The water demand of the mortars was assessed by measuring their flowability and putting it in relation with the water/lime ratio (w/l). The w/l of putties A and B was determined gravimetrically by oven-drying (Table 6). Note that during mortar preparation no extra water was added to the mixture other than that already contained in the lime putties. Differently from the mortars produced using putties, a water quota was added to the mortar made of steam-slaked lime (i.e. a powder) and sand in order to obtain an appropriate workability.

Figure 6 shows the flowability vs w/l plot of mortars based on lime putty (types A and B) and of steam-slaked lime (type C) mortar, prepared by adding various quotes of water. The figure shows that the mortar made with steam-slaked lime needs a $w/l = 0.75–0.77$ to obtain a spread similar to the mortar produced with lime slaked at 20 °C of $w/l = 1.4$; and a $w/l = 0.56–0.63$ to reach a spread similar to the mortar produced with lime slaked at 75 °C ($w/l = 1.3$). Hence, these results suggest that to produce mortars based on steam-slaked lime that have a spread similar to a "traditional" putty-based mortar, only about half the amount of water is required.

Table 6 Calculated w/l values in putty-based mortars, obtained by oven-drying

Lime used	Before drying (g)	After drying (g)	*w/l*
Type A	36.2	15	1.4
Type B	52.5	22.9	1.3

Flexural and compressive tests

Figures 7 and 8 report the results of the flexural and compressive test at maximum load after 28 days of curing, for the mortars produced with lime type 'A', 'B' and 'C'.

Results show that mortars produced with steam-slaked lime ('C') have a significantly higher flexural strength than mortars produced with water-slaked lime at 75°C in flexure. Mortar C shows also a higher mean value in flexural strength with respect to mortar A (made with lime slaked in water at 20 °C) however, the large error bar for mortar C that partially overlaps that of mortar A reduces the significance of these results (Fig. 7). In compression, instead, steam-slaked lime mortars have a strength very similar to the mortars produced with the other types of lime (Fig. 8).

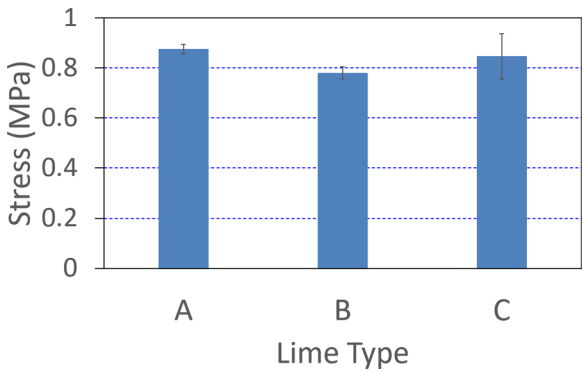

Fig. 8 Compression stress at maximum load at 28 days for the mortars produced with water-slaked lime at 20 °C (**A**) and 75 °C (**B**) and with steam-slaked lime (**C**)

Remarkably, the confidence intervals for the measurements of the steam-slaked lime mortars are much larger than the other two tested mortars, both in flexure and in compression. A possible explanation that accounts for the higher confidence interval of the steam-slaked lime mortar measurements is a higher heterogeneity of these mortars, as it has been observed for uniaxial compression tests performed on natural rocks, where a higher level of heterogeneity was related to a higher coefficient of variation [43]. Such a heterogeneity could have been originated during mixing of the mortar. It is possible that the use of a putty (hydrated lime particles already dispersed in water) allows for a more homogeneous combination with sand during mortar mixing, unlike the use of the steam-slaked lime powder.

Microstructural evolution and carbonation study during mortar hardening

Figures 9, 10 and 11 show the microstructural evolution at 21, 28 and 42 days of mortars produced with lime slaked at 20 °C and 75 °C and steam-slaked, respectively. The images show that, after 21 days of curing, the mortar produced with lime A (at 20 °C) is characterised by a large number of hexagonal portlandite crystals. At 28 days, the number of visible portlandite crystals starts to reduce and some calcite crystals started to appear in the same mortar. At 42 days, portlandite crystals are no longer visible and the microstructure appears more compact. Conversely, in the mortars made with lime B (slaked at 75 °C) and with steam-slaked lime, portlandite crystals are visible throughout the whole curing period, and no significant reduction in porosity can be observed.

Figure 12 shows the results of the phenolphthalein tests for the three types of mortar tested, at 15, 20, 28 and 35 days of curing. The pink colour suggests a pH > 8–9 and, therefore, the presence of portlandite, whereas the

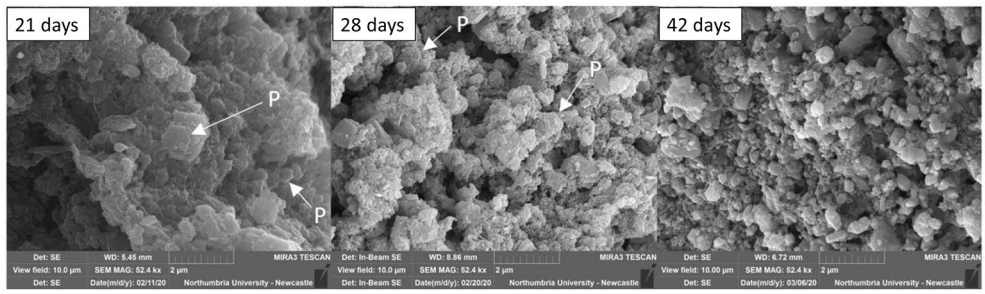

Fig. 9 Microstructural evolution of mortar produced with lime A (slaked 20 °C) at 21, 28 and 42 days of curing

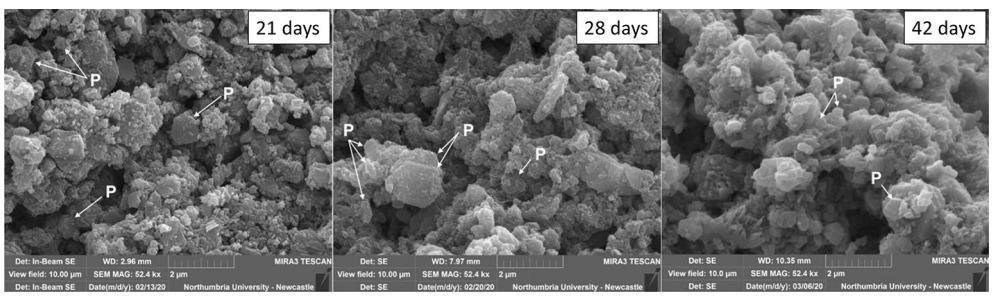

Fig. 10 Microstructural evolution of mortar produced with lime B (slaked 75 °C) at 21, 28 and 42 days of curing

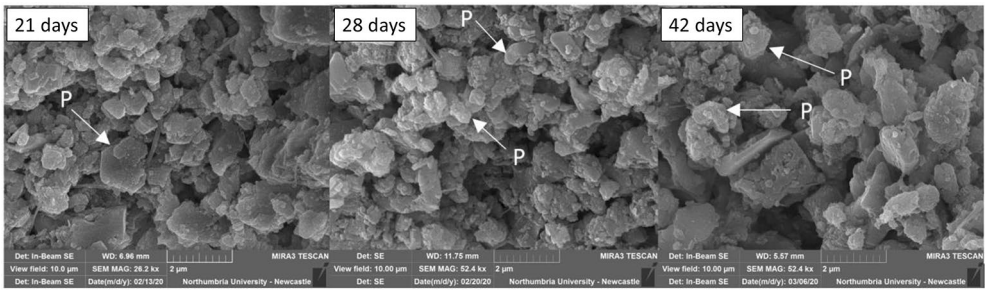

Fig. 11 Microstructural evolution of mortar produced with lime C (steam slaked) at 21, 28 and 42 days curing

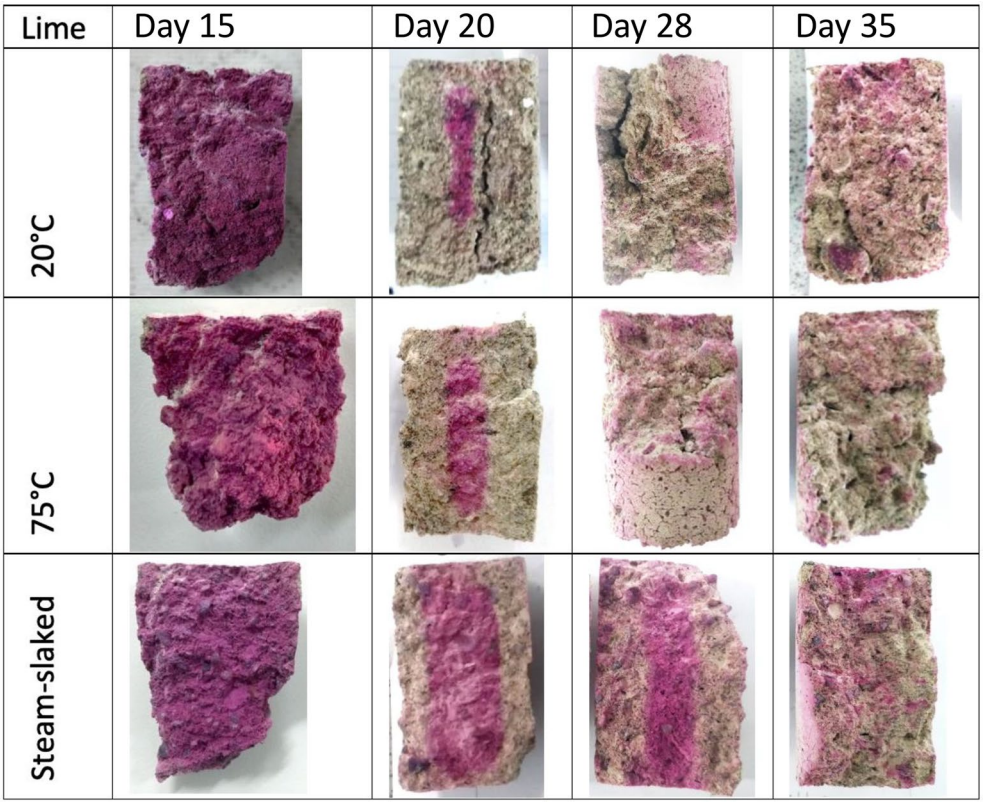

Fig. 12 Comparison between mortars prepared with different types of lime: carbonation front as shown by phenolphthalein sprayed on broken surfaces of carbonated mortar samples

absence of significant pink staining suggests a limited presence of portlandite, which is assumed to be correlated to the conversion of portlandite to calcite through the carbonation reaction. The results show that in the 20 °C water-slaked lime mortar cured for 20 days, the staining front is drastically reduced involving only a few mm along the core of the cylinder; at 28 days, no pink staining is observed on the fractured surface. A similar result is obtained with the 75 °C water-slaked lime mortar, with the only difference that at 28 days the stained area is slightly thicker. The steam-slaked lime mortar shows different results instead. At 28 days, significant staining is still observed in the core of the specimens, and only at 35 days the fracture shows no significant staining.

It is worth noting that, as indicated in the BS EN 14630:2006 [26], the colour change to pink in our samples was recorded within 30 s from spraying the surface. After

that time, a diffused pink colouration slowly appeared on the whole fractured surface, suggesting that in all mortar samples after 35 days of curing only partial carbonation occurred [26].

By comparing the phenolphthalein results with the SEM observations, it can be observed that the analyses are in good agreement in showing that steam-slaked lime mortars are characterised by a slower carbonation rate than 20 °C water-slaked lime mortars. On the other hand, no clear distinction in carbonation rate could be observed with SEM analysis between the 75 °C water-slaked lime mortars and the steam-slaked lime mortars, whereas the phenolphthalein tests clearly show that the steam-slaked lime mortars carbonate significantly slower than the 75 °C water-slaked lime mortars.

Results of the XRD analysis used to investigate the carbonation in mortars are reported in Fig. 13, where diffractograms of the mortar samples after 42 days of curing are shown, and in Fig. 14, where the calcite:portlandite (C/P) ratios of the mortar samples are plotted against the curing time, from 21 to 42 days. The results are in good agreement with the phenolphthalein tests and SEM observations and confirm that the mortar produced with steam-slaked lime has the lowest carbonation rate. Calcite:portlandite ratios measured in the mortars made limes slaked at 20 and 75 °C show the highest values, suggesting a high carbonation rate within these samples compared to the mortar made with steam-slaked lime.

By comparing the results of the carbonation tests at 28 days with the mechanical tests, it is possible to observe to that the flexural strength seems to reflect the carbonation progress. The steam-slaked lime mortar is the least carbonated and shows the highest flexural strength, although with high variation. However, the C/P ratio plot in Fig. 14 shows that at 28 days the carbonation progress is still at a very early stage, with a curve that is still steeply rising, and suggesting that most of the binder is still unconverted $Ca(OH)_2$. This is likely the reason why the results of the mechanical tests are close to each other across the tested mortars.

Since the carbonation reaction is a process that proceeds from the surface towards the core of the material, a weak correlation between specific surface area and carbonation rate has been reported [44]. Hence, considering the microstructural observations in the lime

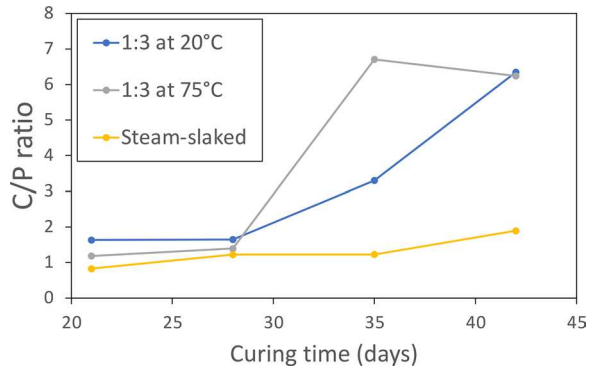

Fig. 14 Calcite:portlandite ratio of different mortar samples at various ages (up to 42 days), exposed to laboratory conditions (20 °C, 40–50% RH)

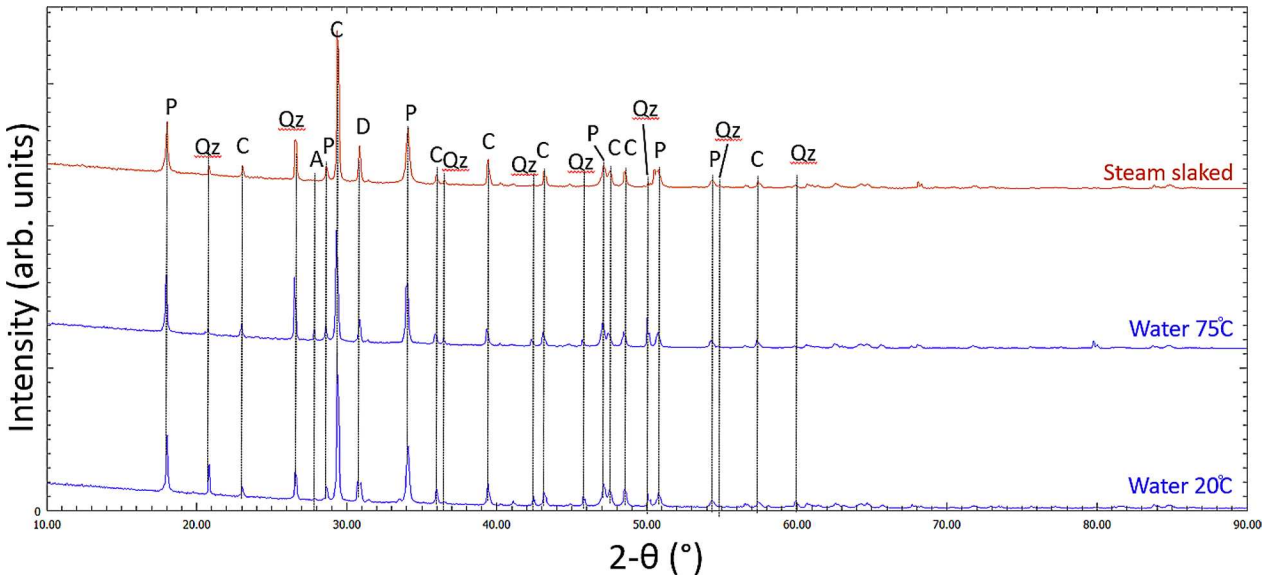

Fig. 13 Diffractograms of mortar samples at 42 days of curing. Keys: P = portlandite; Qz = quartz; C = calcite; A = anorthite; D = dolomite

samples tested in this research (see Sect. "Microstructural and mineralogical characteristics of limes"), it is expected that the carbonation of the mortars tested in this research would follow this order (from the highest carbonation rate to the lowest): steam-slaked > water-slaked at 75 °C > water-slaked at 20 °C. Nevertheless, the data collected suggest a different behaviour. To explain such a behaviour, it is important to take into account the limited RH during curing (see paragraph in Sect. "Mortar preparation and curing conditions") that promoted water evaporation, and the effect of the water content of our mortars on the carbonation rate. It was assessed that water content was the highest in the mortars based on water-slaked lime and the lowest was in the steam-slaked-lime mortar (see parameter W_2 in Table 5). It has been extensively shown that carbonation can only take place within an optimal range of RH% included between 40 and 80 [45]. In such humidity conditions, a molecular-scale layer of water forms on the surface of lime particles, allowing for the dissolution of $Ca(OH)_2$ and CO_2 and subsequent precipitation of $CaCO_3$, but the mortar pores are not fully saturated with water and the diffusion of CO_2 inside the pore network is guaranteed [45–49]. Therefore, it is possible to suggest that in the water-slaked lime mortars, the higher water content facilitated the formation of a water layer where dissolution of $Ca(OH)_2$ and CO_2 could occur, fostering in this manner the carbonation reaction. Carbonation was slowed down in the steam-slaked mortar because of the lower water content that limited the formation of the water molecular layer on the surface of $Ca(OH)_2$ necessary for the dissolution of the involved species.

Overall, this suggest that in the same environmental conditions, the water content was the main driving force in governing the carbonation reaction, rather than the microstructural characteristics of portlandite crystals.

Implications for hot-mixed mortars technology

The reason why the performance of hot-mixed mortars is superior to lime putty mortars is not yet well understood. It is also true that, as stressed by Henry [3] and Midtgaard et al. [8], hot-mixed mortars should not be considered as a panacea for any conservation work, instead their use should be assessed according to the required application and further studies are needed to make hot-mixing a more established practice.

The results of our study allow to clarify some of the characteristics that make hot-mixed mortars attractive to practitioners and conservators, related to the slaking conditions of lime and the role of steam in the hot-mixing process.

Both our SEM and XRD investigations on steam-slaked lime suggest the formation of smaller portlandite crystals than in the water-slaked lime (both at 20 and 75 °C). In a recent study of historic hot-mixed lime plasters [8], it was found through SEM observations of thin sections that in hot-mixed plasters the portlandite crystals are significantly smaller than those of putty-based plasters. This supports the hypothesis that steam slaking plays a major role in determining the characteristics of the binder in hot-mixed mortars.

The smaller portlandite crystal size formed upon steam-slaking is also likely to be responsible for the higher water retention and lower water demand measured in our steam-slaked lime mortars with respect to putty-based lime mortars, as a consequence of a higher colloidal stability of the formers [42]. This finding can also be related to the superior quality of hot-mixed mortars in terms of workability and water retention [4], likely imparted by the presence of smaller portlandite crystals in the binder with respect to putty-based mortars, as a consequence of the steam-slaking occurring during the hot-mixing process.

Furthermore, the same modified mineralogical characteristics of steam-slaked lime are also likely to allow to produce a mortar highly rich in binder, as in hot-mixed mortars. The exceptionally high b/a ratio typical of hot-mixed mortars is regarded as beneficial in terms of both, workability and 'stickiness' of the mix in its fresh state, and enhanced durability in its hardened state [3, 4, 8, 50].

Our mechanical tests showed similar strength of the steam-slaked lime mortars and the water-slaked lime mortars, nonetheless the carbonation progress of the former was less advanced than the latters at time of testing. This suggests that steam-slaked lime mortars potentially outperform water-slaked lime mortars. Long-term tests should be carried out to elucidate the strength development of the mortars and whether steam-slaked lime mortar perform better than water-slaked lime mortars when fully carbonated.

Remarkably, a systematic higher variability was recorded in the steam-slaked mortar samples suggesting a higher structural heterogeneity. It can be argued that such heterogeneity is originated by the presence of lumps in the steam-slaked lime mortars. Indeed, lime lumps are frequently found in historic hot-mixed mortars as a consequence of late hydration and poor mixing of the binder with the aggregate [4, 8, 45, 51–53]. Nevertheless, lime lumps, usually clearly visible either by naked eye or with the aid of optical microscopy, could not be observed in our steam-slaked lime mortars. This leads to two considerations: (i) the procedure of the steam-slaked lime mortar preparation seems to result in a poorer mixing than putty mortars, such to lead to a structural heterogeneity but not enough to lead to the formation of visible pure lime lumps, as in hot-mixed mortars; (ii) the

development of lime lumps in hot-mixed mortars is likely a consequence of the reduced effects of the physical mixing action, rather than by a difference in the microstructural characteristics of the binder as a direct consequence of the steam-slaking process.

Conclusions

In this study, the slaking conditions of lime found according to the traditional technique of hot-mixing were recreated in a simpler system, i.e. by steam-slaking lime in an oven at controlled temperature, in order to isolate the effect of steam, regarded as a crucial factor in the improved properties of hot-mixed mortars, and investigate it as a single variable. The characteristics of lime slaked in steam were compared with those of lime slaked in water at two different temperatures (20 and 75 °C), and the properties of the related mortars were also investigated. Both limes and mortars were characterised at a microstructural level and their carbonation rates were assessed, in an attempt to provide new scientific knowledge on the properties of lime mortars made by the hot-mixing process, and to explain the reasons why these mortars are regarded by many practitioners as superior compared to mortars made with putty. The following conclusions can be drawn from this study:

- Portlandite crystals formed by steam-slaking are different from those formed by water-slaking. In particular, the formers are characterised by a smaller crystallite size, irregular shape and are grouped in assemblies with a micromorphology that resembles that of the unslaked CaO. These differences are likely due to the different reaction path of the hydration process when it occurs at a solid/gas interface compared to solid/liquid interface. The differences between portlandite formed by slaking in room temperature water and portlandite formed after slaking in hot water are not as significant as those between water- and steam-slaked lime. Water-slaked lime has mostly big, rod-like crystals while steam-slaked lime has mostly smaller granular particles.
- Water retention of mortars showed the following trend: steam-slaked lime mortar > > water-slaked at 75 °C lime mortar > water-slaked at 20 °C lime mortar. Such trend is likely the result of the morphological characteristics of portlandite crystals, as the finer-sized crystals observed in the first two limes can impart higher colloidal stability and capacity of water to evenly distribute within the body of the mortar.
- Carbonation rate of the mortars follows the trend (from the lowest to the highest): steam-slaked < < water-slaked at 75 °C < water-slaked at 20 °C. Water content plays an important role in determining the carbonation rate over other factors, such as the portlandite crystals morphology. The higher water content of the mortars made with water-slaked lime favours the carbonation whereas the same process is hindered in the mortar made with steam-slaked lime because of the lower water content.
- Overall, steam-slaked lime is characterised by microstructural properties that allow to produce mortars with higher water retention and that require less water to reach an appropriate consistency than putty-based mortars. These are possibly among the reasons why craftsmen, both nowadays and in the past, preferred hot-mixed mortars over putty-based mortars. Thus, during conservation works the production technology of lime mortars should thoroughly be taken into account and should guide the decision-making process, especially where historic accounts and scientific evidence suggest that hot-mixed mortars were originally employed.

Further research should investigate the effects of steam-slaking lime on the performance and carbonation rate of mortars over a long period of time, as well as the porosity development in steam-slaked lime mortars which is likely one of the major factors affecting carbonation rate.

Abbreviations

γ: Surface tension; b: Width of mechanical tests sample; b:a: Binder to aggregate ratio; C/P: Calcite:portlandite ratio; DI: Deionised; F_c: Maximum load; F_f: Load applied to the middle of the prismatic sample at fracture; h: Height of mechanical tests sample; l: Distance between the flexural test apparatus supports; m_{17}: Mass of the dry filter plate; m_{20}: Mass of the soaked filter plate; m_{21}: Total mass of water in fresh mortar; m_{22}: Mass of dry mortar; m_{23}: Mass of mortar sample; P/P_0: Relative vapour pressure; r: Pore radius; R: Gas constant; R_c: Compressive strength; R_f: Flexural strength; RH: Relative humidity; SEM: Scanning electron microscope/microscopy; T: Temperature; V_m: Molar volume; w/l: Water:lime ratio; W_1: Water fraction; W_2: Water content of mortar; W_3: Mass of water absorbed by the filter plate; W_4: Loss of water from the mortar; WR: Water retention capacity; X_{21}: Water fraction in the putty; X_{22}: Dry mortar fraction; XRD: X-ray diffraction.

Acknowledgements

We acknowledge Tarmac Buxton Lime for providing the quicklime.

Authors' contributions

Conceptualisation: AH, GP and CP. Design of the work: GP and CP. Data acquisition: MCG and CP. Data analysis and interpretation: CP, MCG and GP. Writing—original draft: CP and GLP. All authors read and approved the final manuscript.

Funding

This research was funded by Historic England through the project: "Investigation of the effect of steam slaking on the characteristics of Portlandite crystals in hot-mixed mortars", agreed with Northumbria University on December 2019. Alison Henry of Historic England contributed to the design of the study and in reviewing the manuscript.

Availability of data and materials
All data generated or analysed during this study are included in this published article.

Declarations

Competing interests
The authors declare that they have no competing interests.

Author details
[1]Department of Architecture and Built Environment, Northumbria University, Newcastle upon Tyne NE1 8ST, UK. [2]Historic England, The Engine House, Fire Fly Avenue, Swindon SN2 2EH, UK.

Received: 12 February 2021 Accepted: 6 June 2021
Published online: 16 June 2021

References

1. Forster A. Hot-lime mortars: a current perspective. J Archit Conserv. 2004;10(3):7–27. https://doi.org/10.1080/13556207.2004.10784923.
2. Forster A. Hot-lime mortars: a current perspective. In: Brocklenbank I, editor. Building limes in conservation. Shaftesbuty: Donehead; 2012. p. 251–70.
3. Henry A. Hot-mixed mortars: the new lime revival. Context. 2018;154(5):30–3.
4. Copsey N. Hot mixed lime and traditional mortars. Marlborough: The Crowood Press; 2019.
5. Artis R. Specifying hot-mixed lime mortars. Technical Paper 28. 2018.
6. Schmidt A. Analysis of historic mortar samples in Scotland. 2018.
7. Ponce-Antón G, Zuluaga MC, Ortega LA, Mauleon JA. Multi-analytical approach for chemical-mineralogical characterization of reaction rims in the lime mortars from Amaiur Castle (Navarre, Spain). Microchem J. 2020;152:104303. Available from: https://linkinghub.elsevier.com/retrieve/pii/S0026265X19311567.
8. Midtgaard M, Brajer I, Taube M. Hot-mixed lime mortar: historical and analytical evidence of its use in medieval wall painting plaster. J Archit Conserv. 2020;26(3):235–46. https://doi.org/10.1080/13556207.2020.1785758.
9. Henry A, Stewart J. Practical building conservation. Mortars, renders and plasters. Ashgate Publishing; 2011.
10. Margalha G, Veiga R, Silva AS, De Brito J. Traditional methods of mortar preparation: the hot lime mix method. Cem Concr Compos. 2011;33(8):796–804. https://doi.org/10.1016/j.cemconcomp.2011.05.008.
11. Moropoulou A, Tsiourva T, Bisbikou K, Biscontin G, Bakolas A, Zendri E. Hot lime technology imparting high strength to historic mortars. Constr Build Mater. 1996;10(2):151–9.
12. Válek J, Matas T. Experimental study of hot mixed mortars in comparison with lime putty and hydrate mortars. RILEM Bookseries. 2013;7:269–81.
13. Blamey J, Zhao M, Manovic V, Anthony EJ, Dugwell DR, Fennell PS. A shrinking core model for steam hydration of CaO-based sorbents cycled for CO_2 capture. Chem Eng J. 2016;291:298–305. https://doi.org/10.1016/j.cej.2016.01.086.
14. Serris E, Favergeon L, Pijolat M, Soustelle M, Nortier P, Gärtner RS, et al. Study of the hydration of CaO powder by gas-solid reaction. Cem Concr Res. 2011;41(10):1078–84. https://doi.org/10.1016/j.cemconres.2011.06.014.
15. Ramachandran VS, Sereda PJ, Feldman RF. Mechanism of hydration of calcium oxide. Nature. 1964;201:288–9.
16. Beruto D, Barco L, Belleri G, Searcy AW. Vapor-phase hydration of submicrometer CaO particles. J Am Ceram Soc. 1981;64(2):74–80.
17. Pesce C, Pesce G. Effects of steam slaking on the characteristics of portlandite crystals. In: Proc 39th Cem Concr Sci Conf. 2019;58–61.
18. British Standards. BS ISO 11277:2020 Soil quality—determination of particle size distribution in mineral soil material—method by sieving and sedimentation. 2020.
19. Lordley HE. Water seawage works, Reference Data R-214. 1955.
20. Rodriguez-Navarro C, Ruiz-Agudo E, Ortega-Huertas M, Hansen E. Nanostructure and irreversible colloidal behavior of $Ca(OH)_2$: implications in cultural heritage conservation. Langmuir. 2005;21(24):10948–57.
21. Rodriguez-Navarro C, Ruiz-Agudo E, Burgos-Cara A, Elert K, Hansen EF. Crystallization and colloidal stabilization of $Ca(OH)_2$ in the presence of nopal juice (Opuntia ficus indica): implications in architectural heritage conservation. Langmuir. 2017;33(41):10936–50.
22. Rosell JR, Haurie L, Navarro A, Cantalapiedra IR. Influence of the traditional slaking process on the lime putty characteristics. Constr Build Mater [Internet]. 2014;55:423–30. https://doi.org/10.1016/j.conbuildmat.2014.01.007.
23. Navrátilová E, Tihlaříková E, Neděla V, Rovnaníková P, Pavlík J. Effect of the preparation of lime putties on their properties. Sci Rep. 2017;7(1):1–9.
24. British Standards Institution. BS EN 196-1:2016 methods of testing cement. 2016.
25. Hall WH. X-ray line broadening in metals [3]. Proc Phys Soc A. 1949;62(11):741–3.
26. British Standards Institution. Products and systems for the protection and repair of concrete structures—test methods—determination of carbonation depth in hardened concrete by the phenolphthalein method. BS EN 146302006. 2006.
27. BS EN 459-2: BSI Standards Publication Building lime Part 2: Test methods. 2010.
28. Hendrickx R, Minet J, Van Balen K, Van Gemert D. Workability of mortars with building lime: assessment by a panel of masons versus lab testing. In: International Brick & Block Masonry Conference. 2008.
29. British Standards Institution. BS EN 12350-5:2019 Testing fresh concrete - Flow table test. 2019;18.
30. Miller J, Miller JC. Statistics and chemometrics for analytical chemistry. Pearson Education, Limited; 2018.
31. Witoon T. Characterization of calcium oxide derived from waste eggshell and its application as CO_2 sorbent. Ceram Int. 2011;37(8):3291–8.
32. Kavosh M, Patchigolla K, Anthony EJ, Oakey JE. Carbonation performance of lime for cyclic CO_2 capture following limestone calcination in steam/CO_2 atmosphere. Appl Energy. 2014;131:499–507. https://doi.org/10.1016/j.apenergy.2014.05.020.
33. Moropoulou A, Bakolas A, Aggelakopoulou E. The effects of limestone characteristic, granulation and calcination temperature to the reactivity of quicklime. Cem Concr Res. 2001;31:633–9.
34. Kumar GS, Ramakrishnan A, Hung Y-T. Lime calcination. In: Advanced physicochemical treatment technologies handbook of environmental engineering. Humana Press; 2007.
35. Seo JH, Park SM, Yang BJ, Jang JG. Calcined oyster shell powder as an expansive additive in cement mortar. Materials (Basel). 2019;12(8):1322.
36. Boynton RS. Chemistry and technology of lime and limestone. New York: Wiley; 1980.
37. Molinder R, Comyn TP, Hondow N, Parker JE, Dupont V. In situ X-ray diffraction of CaO based CO_2 sorbents. Energy Environ Sci. 2012;5(10):8958–69.
38. Bajpai P. Colloid and surface chemistry. In: Biermann's handbook of pulp and paper. 2018. p. 381–400.
39. Elert K, Rodriguez-Navarro C, Pardo ES, Hansen E, Cazalla O. Lime mortars for the conservation of historic buildings. Stud Conserv. 2002;47(1):62–75.
40. Thomson ML. Plasticity, water retention, soundness and sand carrying capacity: what a mortar needs. Int RILEM Work Hist Mortars Charact Tests Paisley, Scotland, 12th–14th May 1999. 2000;163–72.
41. Razzaghian Ghadikolaee M, Habibnejad Korayem A, Sharif A, Ming Liu Y. The halloysite nanotube effects on workability, mechanical properties, permeability and microstructure of cementitious mortar. Constr Build Mater. 2020;120873. Available from: http://www.sciencedirect.com/science/article/pii/S0950061820328786.
42. Hansen EF, Rodríguez-Navarro C, Balen K. Lime putties and mortars. Stud Conserv. 2008;53(1):9–23. https://doi.org/10.1179/sic.2008.53.1.9.
43. Lan HC, Martin D, Bo H. Effect of heterogeneity of brittle rock on micromechanical extensile behavior during compression loading. J Geophys Res Solid Earth. 2010;115.
44. Cizer Ö, Van Balen K, Elsen J, Van Gemert D. Real-time investigation of reaction rate and mineral phase modifications of lime carbonation. Constr Build Mater. 2012;35:741–51.

45. Veiga R. Air lime mortars: What else do we need to know to apply them in conservation and rehabilitation interventions? A review. Constr Build Mater. 2017;157:132–40.
46. Shih S-M, Ho C-S, Song Y-S, Lin J-P. Kinetics of the reaction of $Ca(OH)_2$ with CO_2 at low temperature. Ind Eng Chem Res. 1999;38(4):1316–22. https://doi.org/10.1021/ie980508z.
47. Steiner S, Lothenbach B, Proske T, Borgschulte A, Winnefeld F. Effect of relative humidity on the carbonation rate of portlandite, calcium silicate hydrates and ettringite. Cem Concr Res. 2020;135:106116. Available from: http://www.sciencedirect.com/science/article/pii/S0008884620301204.
48. El-Turki A, Ball RJ, Allen GC. The influence of relative humidity on structural and chemical changes during carbonation of hydraulic lime. Cem Concr Res. 2007;37(8):1233–40. Available from: http://www.sciencedirect.com/science/article/pii/S0008884607001196.
49. Cizer Ö, Rodriguez-Navarro C, Ruiz-Agudo E, Elsen J, Van Gemert D, Van Balen K. Phase and morphology evolution of calcium carbonate precipitated by carbonation of hydrated lime. J Mater Sci. 2012;47(16):6151–65.
50. Malinowski ES, Hansen TS. Hot lime mortar in conservation—repair and replastering of the façades of Läckö Castle. J Archit Conserv. 2011;17(1):95–118.
51. Elsen J. Microscopy of historic mortars—a review. Cement Concrete Res. 2006;36:1416–24.
52. Loureiro AMS, da Paz SPA, Veigado MR, Angélica RS. Investigation of historical mortars from Belém do Pará, Northern Brazil. Constr Build Mater. 2020;233:117284.
53. Pesce C, Leslie AB, Henry A, David J, Pesce GL. The use of dolomitic lime in mortar samples from a 15th-century buttress of York Minster (York, UK). In: 5th Historic Mortars Conference. 19–21 June 2019, Pamplona, Spain. 2019. pp. 986–96.

Publisher's Note